PCCP

PAPER

View Article Online
View Journal

Cite this: DOI: 10.1039/c3cp54364a

Polarization control of metal-enhanced fluorescence in hybrid assemblies of photosynthetic complexes and gold nanorods

Ł. Bujak,[a] M. Olejnik,[a] T. H. P. Brotosudarmo,[b] M. K. Schmidt,[c] N. Czechowski,[a] D. Piatkowski,[a] J. Aizpurua,[c] R. J. Cogdell,[d] W. Heiss[e] and S. Mackowski*[a]

Received 15th October 2013,
Accepted 17th March 2014

DOI: 10.1039/c3cp54364a

www.rsc.org/pccp

Fluorescence imaging of hybrid nanostructures composed of a bacterial light-harvesting complex LH2 and Au nanorods with controlled coupling strength is employed to study the spectral dependence of the plasmon-induced fluorescence enhancement. Perfect matching of the plasmon resonances in the nanorods with the absorption bands of the LH2 complexes facilitates a direct comparison of the enhancement factors for longitudinal and transverse plasmon frequencies of the nanorods. We find that the fluorescence enhancement due to excitation of longitudinal resonance can be up to five-fold stronger than for the transverse one. We attribute this result, which is important for designing plasmonic functional systems, to a very different distribution of the enhancement of the electric field due to the excitation of the two characteristic plasmon modes in nanorods.

Introduction

Metallic nanoparticles are suitable for controlling and manipulating optical fields at the nanoscale through collective excitation of free electrons called plasmons.[1] Plasmon-induced modifications of the optical properties of fluorophores have been implemented in many research areas including optoelectronics,[2,3] biosensors,[4,5] artificial photosynthesis,[6,7] and high-resolution spectroscopy.[8–10] This diversity of applications is stimulated by a variety of morphologies of fabricated metallic nanoparticles, controlled through proper conditions in chemical reactions or nanofabrication techniques. As a result, it is possible to synthesize gold nanospheres, nanorods, nanowires, nanostars, nanocubes, nanoshells, *etc.*[11–13] The variation in sizes and shapes has a profound effect on the plasmonic properties of the nanostructures obtained: while gold nanospheres of radius up to tens of nanometers feature a single resonance at around 530 nm, in the case of nanorods, two dominant resonances appear intuitively assigned to the charge oscillations along the two specific axes of the nanorod. Importantly, the absolute strengths of the resonances as well as the spectral separation between them can be, to a large degree, tuned by changing the aspect ratio of the nanorods during synthesis.[11] A typical preparation yields gold nanorods with one resonance between 530 nm and 600 nm and the other resonance between 650 nm and up to 1200 nm.[14] Importantly, the intensity of the absorption in the band attributed to the latter, long wavelength resonance, is always much larger.

Spectroscopy of hybrid nanostructures composed of metallic nanorods and fluorophores has provided remarkable insights into the interactions present in such systems.[15–18] It has been shown for instance that plasmon excitations in metallic nanorods lead to the enhancement of the single oxygen emission[16] and the fluorescence enhancement of fluorophores conjugated directly to the ends of the nanorods.[15] While studies exploiting the interaction with one of the two resonances of metallic nanorods have been carried out, limitations associated with the narrow absorption and emission bands of fluorophores, as compared to the splitting between the two resonances of a metallic nanorod, inhibit simultaneous analysis of the impact that both resonances have on a single absorbing–emitting system. Multichromophoric assemblies, such as light-harvesting systems,[19] provide a way to overcome this obstacle as they feature broad absorption bands spanning over the whole visible spectrum into the near-IR. Recently important advancements in fabrication of hybrid nanostructures that involve photosynthetic systems and metallic nanoparticles have been reported.[20–25] In particular, effects of plasmon excitations in silver nanostructured films and in spherical nanoparticles on the absorption and emission of several

[a] *Institute of Physics, Faculty of Physics, Astronomy and Informatics, Nicolaus Copernicus University, Grudziadzka 5, 87-100 Torun, Poland. E-mail: mackowski@fizyka.umk.pl*
[b] *Ma Chung Research Center for Photosynthetic Pigments, Ma Chung University, Malang, Indonesia*
[c] *Donostia International Physics Center DIPC and Centro de Física de Materiales CSIC-UPV/EHU, Donostia-San Sebastián, 20018, Spain*
[d] *Institute of Molecular Cell and Systems Biology, University of Glasgow, Glasgow, UK*
[e] *Institut für Halbleiter-und Festkörperphysik, Universität Linz, 4040 Linz, Austria*

light-harvesting and photosynthetic complexes have been studied. For geometries, where monodispersed metallic nanoparticles were coupled with light-harvesting complexes with precise control of their separation, a strong increase of absorption or emission has been observed.[24] In contrast, biochemical conjugation facilitating coupling between metallic nanoparticles and photosynthetic complexes, led to efficient quenching of fluorescence.[23] Finally, in the context of possible photovoltaic applications of biomimetic hybrid systems, inhomogeneous assemblies of metallic nanoparticles have been demonstrated as a promising way for spectral broadening of absorption enhancement.[23] We therefore consider metallic nanorods that feature two plasmon resonances, as model nanostructures, for investigating the spectral dependence of plasmon excitation upon the optical properties of fluorophores.

In this work we investigate the optical properties of a hybrid nanostructure composed of a light-harvesting complex LH2 from purple bacteria and gold nanorods. The particular advantage of the LH2 complex in comparison to standard fluorophores is the presence of absorption bands, both in the visible and infrared spectral range, to which we tune the resonances of the synthesized nanorods. In this way, by using the LH2 complexes, we overcome the limitation of most fluorophores and organic dyes, which feature spectrally narrow optical spectra, thus inhibiting simultaneous probing of fluorescence enhancement of the same emitter at excitations resonant with both, transverse and longitudinal, plasmon resonances in metallic nanorods. The separation between the nanorods and the light-harvesting complexes is defined by silica layers of fixed thickness, thus allowing us to control the strength of the coupling between the fluorophores and nanorods. The results of fluorescence imaging carried out for LH2 complexes excited at laser wavelengths corresponding to both plasmon resonances of the nanorods demonstrate that the enhancement and its variation with the spacer thickness depends on the excitation wavelength. It is as large as five-fold stronger for the resonance associated with the long axis of the nanorod. Experimental data are reproduced by rigorous calculation of the electric field generated by Au nanorods illuminated with both longitudinal and transverse polarizations. These results, which are of fundamental importance in the context of understanding the mechanism of plasmon induced effects in hybrid nanostructures, can also have implications towards designing plasmonics-based architectures for photovoltaic applications, in particular in the near-infrared spectral region.

Materials and methods

The LH2 complexes from *Rps. palustris* were prepared as described elsewhere.[26] They were stored in Tris buffer with 0.1% lauryldimethylamine *N*-oxide (LDAO). Gold nanorods were synthesized using a seed-mediated growth method[27] and stored in aqueous solution. Briefly, first Au seeds were prepared by mixing cetyltrimethylammonium bromide (CTAB) solution (4.7 ml, 0.1 M) with 25 μl of 0.05 M $HAuCl_4$. Next, 0.3 ml of 0.01 M $NaBH_4$ was added to the stirred solution, which resulted in appearance of brownish yellow color to the mixture. Vigorous stirring of the seed solution was continued for another 3 min. The synthesis of Au nanorods followed immediately, with the reaction carried out in aqueous solution, under soft conditions of atmospheric pressure and near room temperature. Appropriate quantities and molarities of CTAB (150 ml, 0.1 M), $HAuCl_4$ (1.5 ml, 0.05 M), L-ascorbic acid (1.2 ml, 0.1 M), 0.01 M $AgNO_3$ (1.6 ml, 1.8 ml, 2 ml) and Au seeds (360 μl) were added one by one to a flask, followed by gentle mixing. Due to the presence of ascorbic acid, which is a mild reducing agent, the color of the mixture changed from dark yellow to colorless. After addition of the Au seed solution, the mixture was put into a water bath and kept at a constant temperature of 28 °C for 2 hours. The products were separated from the unreacted substrate and spherical particles by centrifugation at 9.000 rpm for 60 minutes. The supernatant was removed using a pipette and the precipitate was redissolved in pure water. The average size of the nanorods was 15 nm in diameter and 55 nm in length, as determined using scanning electron microscopy.

In order to assemble a hybrid nanostructure composed of LH2 complexes and gold nanorods we combine spin-coating with electron beam evaporation in vacuum. First the Au nanorods were dispersed on clean glass coverslips using spin-coating. In this way, since the nanorods were diluted in water, a sub-monolayer of the nanoparticles is formed on the glass surface. Next, we cover the layer of Au nanorods with an SiO_2 spacer. The thickness of the spacer layer was varied from 5 to 30 nm, as measured by a microbalance and cross checked by atomic force microscopy. The dielectric layer provides a way to control the interaction between plasmon excitations in Au nanorods and pigments in the LH2 complex. In the final step, on top of the SiO_2 surface we spin-coated the LH2 photosynthetic complexes embedded in a polymer matrix (PVA).

Absorption spectra of both, LH2 complexes and Au nanorod solutions, were obtained using a Perkin Elmer Lambda 2 spectrophotometer. The spectra were recorded at room temperature in the range 350–1100 nm, using a quartz cuvette with 1 cm optical path. Fluorescence properties of the hybrid nanostructures assembled of LH2 complexes and Au nanorods were examined using a home-built scanning confocal fluorescence microscope.[28] This system is based on a long working distance microscope objective LMPlan 50× (Olympus) with a numerical aperture of 0.5. The sample was placed on a XYZ piezoelectric stage (Physik Instrumente), which allows for precise translation of the sample. For excitation we use two lasers with energies (λ = 556 nm and λ = 808 nm) corresponding to the plasmon resonances of the gold nanorods. Although the polarization of the excitation laser was not controlled, the strong spectral selectivity of plasmonic resonances in the nanorods results in selective excitation of longitudinal plasmons with 808 nm excitation and the transverse ones with 556 nm excitation. For both lasers the excitation power was 2 μW focused on a 1 μm spot on the sample. Fluorescence of the LH2 complexes, collected in back-scattering geometry, was focused on a confocal pinhole (150 μm) before passing the filters – a longpass filter (Chroma HQ850LP) and a bandpass filter (Chroma D880/40m). Fluorescence maps were obtained by correlating the movement of the piezoelectric stage

and the acquisition of fluorescence spectra using an avalanche photodiode (Perkin Elmer SPCM-AQRH-14). The emission spectra were dispersed using an Amici prism and measured using a CCD camera (Andor iDus DV 420A-BV).

Results and discussion

The absorption spectrum of the LH2 solution is compared with the one recorded for the Au nanorods shown in Fig. 1a. The spectra are scaled for better comparison. The pigment organization in the LH2 complex and its relation to the absorption bands has been discussed previously.[29] The absorption spectrum features two prominent bands at 800 nm and 850 nm, which originate from the two rings of bacteriochlorophyll (BChl) molecules – a strongly coupled ring of 18 BChl molecules and a weakly coupled ring of 9 BChl molecules. In addition to the BChl molecules, the LH2 complex also contains 9 carotenoid molecules, which contribute to the absorption spectrum through a broad band between 400 nm and 550 nm, thus partially filling the absorption gap. The fluorescence of LH2 (Fig. 1a) has an excitonic character and originates from the strongly coupled B850 ring.[30] The absorption spectrum of Au nanorods features two bands that we attribute to transverse and longitudinal plasmon excitation, at 550 nm and 800 nm, respectively. It also features a small band at 520 nm, presumably due to the presence of some scarce spherical or cubic nanoparticles. The hybrid nanostructure is therefore tailored to match the energies of both plasmon resonances with absorption bands of the light-harvesting complex. In this way we can study the impact of both plasmons on the optical properties of the LH2 complex. In Fig. 1b we show the scanning electron microscope image of a surface covered sparsely with Au nanorods. In the inset an image obtained with higher magnification is displayed. Although in the absorption spectrum we observe a high-energy band that could be attributed to spherical or cubic nanoparticles, the scanning electron microscope images contain essentially only nanorods. The substrates studied in this work were prepared using an analogous approach, therefore we expect the surface density of the nanorods in samples with silica spacers to be comparable.

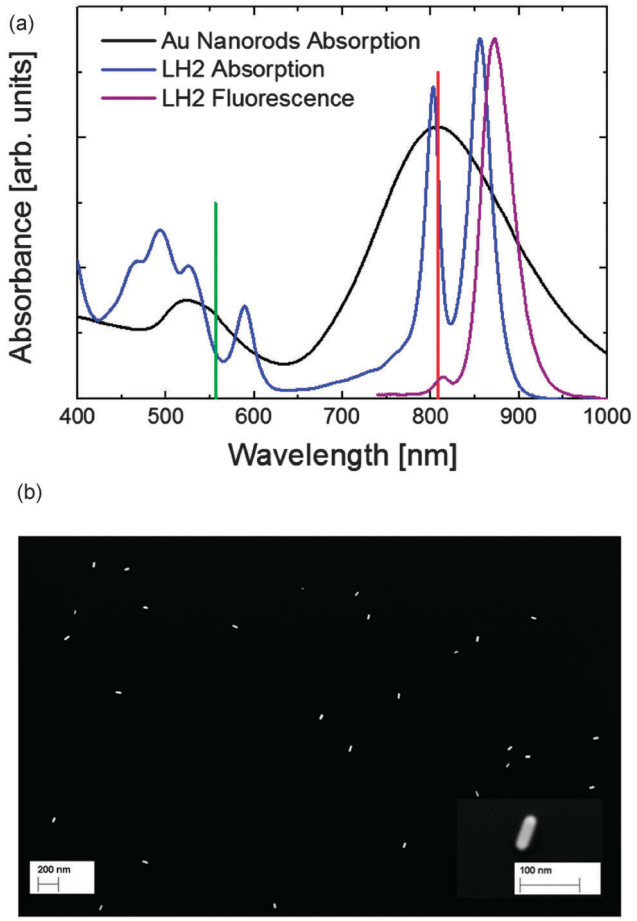

Fig. 1 (a) Absorption spectra of the LH2 complexes in solution (blue) and gold nanorods (black) used to assemble a hybrid nanostructure. Purple line represents fluorescence of the LH2 complexes excited at 556 nm. Vertical lines correspond to the excitation energies at 556 nm and 808 nm. (b) Scanning electron microscope image obtained for Au nanorods dispersed on a substrate. In the inset magnification of a single nanorod is shown.

The experimental approach to determine the distance dependence of the enhancement of the LH2 fluorescence due to coupling with both plasmon resonances in the Au nanorods is based on collecting fluorescence maps for structures with varied thickness of the SiO_2 spacer layer. Two excitation energies of 556 nm and 808 nm were used in order to match the plasmon energies of the Au nanorods (marked by vertical lines in Fig. 1). Using these two excitation wavelengths we also diminish any possible influence of nanoparticles other than nanorods, *i.e.* those responsible for the 520 nm band in the absorption spectrum (Fig. 1). Namely, plasmon resonances in such nanostructures are, in addition to strong polarization selection, beyond our excitation wavelengths. During the experiment, fluorescence maps were collected using an avalanche photodiode coupled to a piezoelectric stage. The stepsize of the stage was 0.5 μm, the size of the map is 50 × 50 μm and photons were acquired for 0.01 s per point. Before the maps were collected, we recorded fluorescence spectra of the LH2 complexes deposited on the Au nanorods. For all studied samples with varied thickness of the SiO_2 spacer, the spectra were identical in shape to those of the LH2 complexes in solution. This indicates that the LH2 complexes are intact and that the functionality of these light-harvesting complexes is not hampered in any way by coupling to metallic nanoparticles.

In Fig. 2 we show maps of the LH2 fluorescence intensity that were obtained for both excitation wavelengths for the structures with a silica spacer of 5 nm, 15 nm, and 30 nm. It is important to emphasize that the maps for a given spacer were measured always for the same sample area for both excitation wavelengths. In this way we can straightforwardly compare the obtained distributions of the fluorescence intensity. The correspondence between the maps, most clearly seen in Fig. 2 for a 30 nm-thick spacer structure, confirms that the maps were acquired for the same region of the sample. For each spacer a set of five pairs of maps were measured in order to obtain statistical information about the fluorescence intensity and the ratio thereof between both excitation wavelengths.

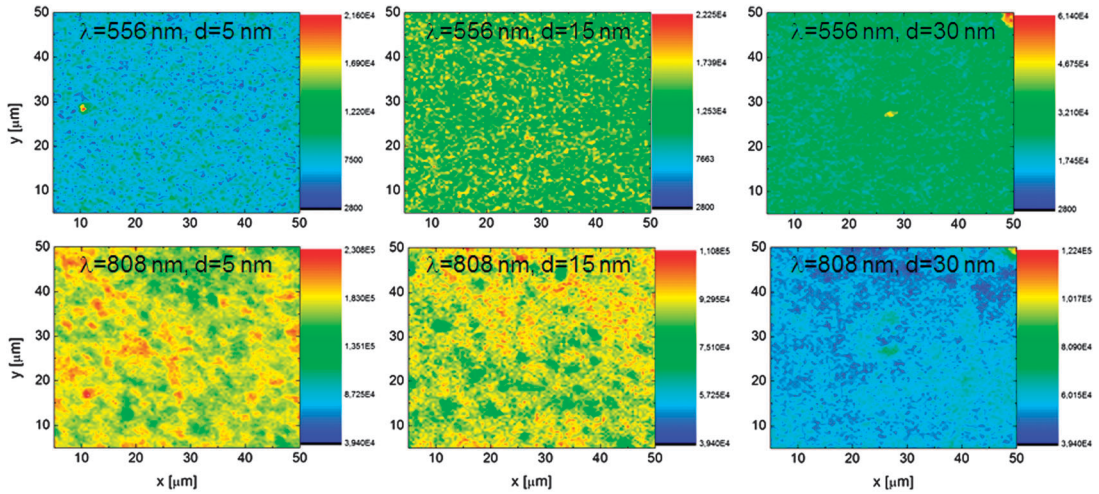

Fig. 2 Maps of fluorescence intensity obtained for LH2 complexes deposited on Au nanorods spaced by 5 (left), 15 (middle), and 30 nm (right). The intensity scale for all maps was set to enhance the contrast. The upper row corresponds to the excitation at 556 nm, while lower row corresponds to the excitation at 808 nm.

There are important qualitative observations regarding the fluorescence maps shown in Fig. 2. In the case of the thickest spacer (30 nm) the maps recorded at both excitation wavelengths (556 and 808 nm) show rather homogeneous distribution of the LH2 fluorescence intensity. As the thickness of the silica spacer is reduced, different distributions of the fluorescence intensities are observed and these differences become more apparent between maps recorded for 556 and 808 nm excitations. Reduction of the SiO_2 spacer increases the influence of the electric field induced in the nanorods upon the pigments in the LH2 complexes. The strength of the interaction becomes thus more sensitive to any variations of the spacer thickness. This leads to a significant increase of inhomogeneity of fluorescence intensities, resulting in less uniform fluorescence maps (Fig. 2). Similar dependencies are generally observed for all sets of fluorescence maps collected for any particular spacer thickness. The increase of fluorescence intensity distribution upon coupling with metallic nanoparticles is frequently observed in hybrid nanostructures[20,21] and it originates predominantly from variations of the electric field strength due to small variations of the distance between metallic nanoparticles and fluorophores, due to different orientations of the fluorophores with respect to the metallic nanoparticles, or due to formation of hot spots between coupled metallic nanoparticles.[31]

The apparent distribution of the fluorescence intensity for hybrid nanostructures emphasizes the approach applied in this work that is based on measuring and analyzing fluorescence intensity maps instead of the previously applied random scanning of the sample surface.[24] In contrast to acquiring a relatively small number of fluorescence spectra, we obtain in this way an instant information about the fluorescence intensity out of 10^4 points in a single experiment. The comparison between the results obtained for both excitation wavelengths is also better supported from the statistical point of view, in comparison with a case, where for instance intensities for hundred spots across the sample were obtained for the wavelengths corresponding to both plasmon resonances in the Au nanorods.

In order to evaluate the plasmon induced enhancement of the LH2 fluorescence due to coupling with longitudinal and transverse modes in the nanorods, we calculated histograms of intensities collected for each map. The dependence of the emission intensity upon the thickness of the SiO_2 spacer for both excitation wavelengths is displayed in Fig. 3. Data measured for spacer thicknesses of 30 nm, 20 nm, and 5 nm are shown. The red and green histograms correspond to intensities measured for excitation at 808 nm and 556 nm, respectively. Each of the six histograms displayed in Fig. 3 has been obtained from a single fluorescence map. In this way in a single experiment we acquire information about interactions between LH2 complexes and Au nanorods out of a large sample area. It is also important to note that the histograms plotted for the same thickness of the silica spacer were obtained for the same area of the sample (in analogy to

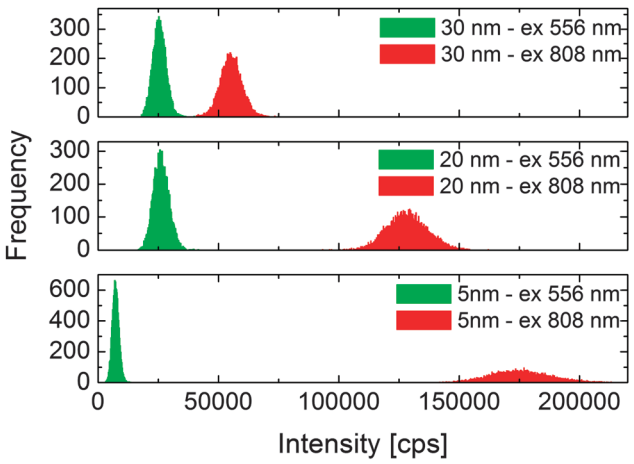

Fig. 3 Examples of histograms extracted from the fluorescence maps measured for indicated excitation conditions and for structures with varied thickness of the spacer.

the fluorescence maps shown in Fig. 2). Therefore, we can directly relate the results to one another. The comparison of fluorescence intensity distributions for structures with varied thickness of the dielectric spacer points towards substantial differences in the strength of plasmon induced enhancement for the two excitation wavelengths. Indeed, should the distribution of fluorescence intensity originates solely from the inhomogeneities related to LH2 concentration variation across the sample surface, the resultant broadening for both excitation wavelengths would be identical and independent of the thickness of the silica spacer. We find that in the case of 556 nm excitation, which is resonant with the transverse plasmon in the Au nanorods, the enhancement is minimal and we observe a rapid decrease of the emission intensity for thinner spacers. In contrast, when the longitudinal plasmon is excited in the Au nanorods using the 808 nm laser, the results show a pronounced increase in intensity. Even for the thinnest spacer of 5 nm, the average fluorescence intensity is still larger than for the reference structure (30 nm-thick spacer). We consider the structure with a 30 nm-thick silica spacer as a reference, as for such large separation between metallic nanoparticles and LH2 complexes, the influence of plasmonic excitations in the Au nanorods is negligible.[24] The histograms also display significant differences in the distribution of intensities for structures with different spacers, excited with both excitation wavelengths. Nevertheless, the distributions are still narrower than the estimated variations of average fluorescence intensities as a function of spacer thickness.

Statistically relevant determination of the enhancement factors and their dependence on the excitation energy was obtained by analyzing all five pairs of fluorescence maps obtained for each spacer thickness. In Fig. 4a we present the average intensities of the LH2 emission measured for both excitation wavelengths as a function of the spacer layer thickness. Black and red symbols correspond to the values obtained at the 556 nm and 808 nm excitation wavelengths, respectively, while green symbols are the data for the 556 nm excitation multiplied by a factor of 5. The variation of the fluorescence intensity observed for the excitation wavelength that corresponds to the longitudinal resonance of the nanorod exhibits a maximum at 10 nm thickness of the silica layer. The dependence measured when the hybrid nanostructure is excited with the 556 nm wavelength is qualitatively similar. The fluorescence intensity increases first with reduction of the spacer thickness, and then it starts to gradually decrease as the spacer gets thinner. In contrast to the situation observed for the 808 nm excitation, however, the maximum of the fluorescence intensity appears at 20 nm.

These results demonstrate that the enhancement of the fluorescence depends critically upon the excitation of either longitudinal or transverse plasmon resonance in the nanorods. The effect of spectral dependence of the fluorescence intensity is displayed in Fig. 4b, where we plot a ratio of the average intensities measured as a function of the spacer thickness for both excitation energies. While for the structure with a 30 nm-thick spacer the ratio is approximately 5, as for LH2 complexes uncoupled to metallic nanoparticles, it reaches a

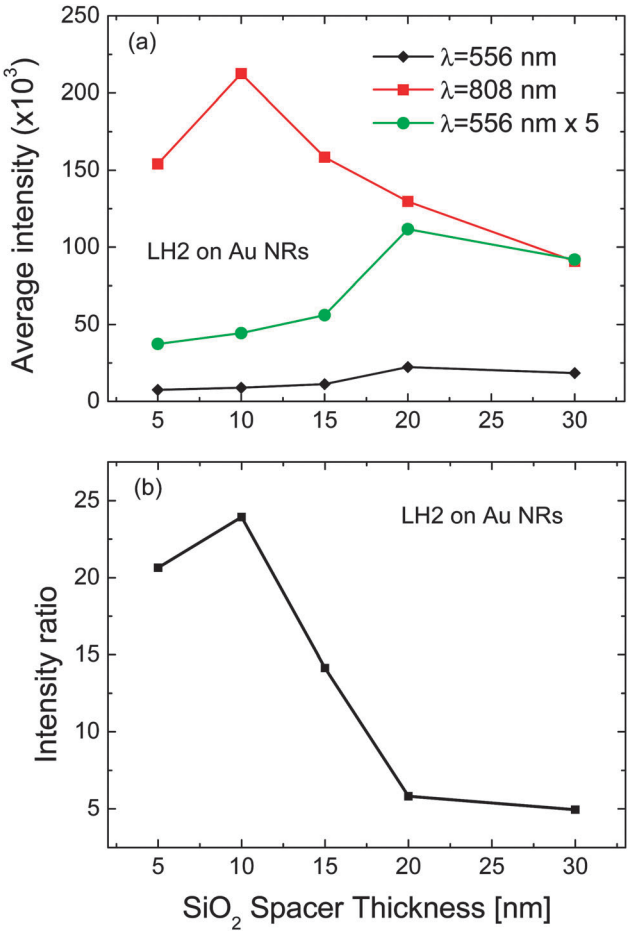

Fig. 4 (a) Averaged intensities of the LH2 fluorescence as a function of the spacer thickness. Red and black curves indicate excitation at 808 nm and 556 nm, respectively. A green line was obtained by multiplying the data obtained for the excitation at 556 nm by a factor of 5. (b) The ratio of the average intensity estimated for both excitation energies of 556 nm and 808 nm.

factor of 20 for the spacer of 10 nm. This demonstrates that in the case of hybrid nanostructures composed of nanorods or even more complex metallic nanoparticles showing multiple plasmon resonances, the enhancement values can vary substantially, depending upon the actual geometry and excitation conditions. As mentioned above, as the polarization of the excitation laser was not controlled, selective excitation of longitudinal (transverse) plasmons with excitation at 808 nm (556 nm) is enabled by strong spectral selectivity of plasmonic resonances in the nanorods. It might therefore be possible to achieve even larger values of fluorescence enhancement for hybrid nanostructures composed of aligned nanorods.

In order to understand the above results, we have performed numerical calculations of the plasmon excitation in the investigated system. In the weak coupling regime applicable here, the rate of an excitation of a molecule by light is proportional to the squared intensity of the electric field calculated at the frequency corresponding to the dipolar transition of the molecule. We thus estimate the average excitation enhancement of an evenly distributed layer of molecules, due to the presence of

the nanorod, by the ratio of the squared intensities of the electric fields in the systems with and without the nanorod, averaged over the surface S where the molecules are distributed. The excitation enhancement factor κ is therefore defined as:[32,33]

$$\kappa = \frac{\left\langle \left|\mathbf{E}_{\mathrm{tot,NR}}\right|^2 \right\rangle_S}{\left|\mathbf{E}_{\mathrm{tot,ref}}\right|^2},$$

where $\langle \cdots \rangle_S$ denotes an average over S, $\mathbf{E}_{\mathrm{tot,NR}}$ and $\mathbf{E}_{\mathrm{tot,ref}}$ are the total electric fields in S induced by the incident light, calculated in the presence and absence of the nanorod structure, respectively. Since the experiments were performed on a surface with very low surface density of nanorods of about one per 0.25 μm^2, we limit our calculations to a contribution from a single nanorod.

The enhancement of the fluorescence under continuous wave illumination is described as the outcome of both the enhancement of the excitation rate, and the modification of the quantum efficiency of the emitters. In our work, we neglect the latter effect, as the modification of the quantum efficiencies of emitters is very weak due to the presence of the spacer and the small size of the nanorod. We can therefore expect to reproduce the data shown in Fig. 4 by numerical calculations of the excitation enhancement rates.

We have performed the calculations of $\mathbf{E}_{\mathrm{tot,NR}}$ and $\mathbf{E}_{\mathrm{tot,ref}}$ using a commercial-grade Maxwell's equation solver based on the finite-difference time-domain method.[34] The nanorod was modeled as a cylinder capped with two hemispheres, with radii set to 7.5 nm and a total length of 55 nm, placed on top of a bulk silica substrate. The spacer comprises a flat layer of silica around the nanorod, and a silica coating on the top of the surface of the nanorod (see schematics pf the system adopted in Fig. 5a). The refractive indices of the gold and silica were taken from ref. 35. The surface S was defined as the top surface of the dielectric spacer. For the excitation of the longitudinal (transverse) dipolar plasmonic mode in the nanorod, the wavelength of the incident light was set to 800 nm (550 nm), and its polarization – parallel (perpendicular) to the symmetry axis of the nanorod. The wavelengths used for calculation are slightly different from the experimental values, but taking into account the broadening of bot plasmon resonances of the gold nanorods, this approximation is justified and should not influence the theoretical results. In Fig. 5b we show maps of the field enhancement $|\mathbf{E}_{\mathrm{tot,NR}}/\mathbf{E}_{\mathrm{tot,ref}}|^2$, calculated on the surface of a dielectric spacer of 9 nm thickness. The wavelengths and polarizations of the incident light are marked in the plots. The maps of near field enhancement maps are characteristic of the dipolar longitudinal and transverse resonances, with the former focusing fields near the tips of the nanorod, and the latter along its entire length. These very different geometric properties of the field enhancements should be reflected in the dependence of the enhancement factors on the spacer thickness.

Furthermore, to trace the spectral position of the resonances against the changing spacer thickness, we have calculated the field enhancement at arbitrary positions indicated by black crosses in Fig. 5b. The results are shown in Fig. 5c and indicate that while the spectral position of the transverse resonance (left panel) is independent of the spacer thickness, the longitudinal resonance (right panel) is very sensitive to the thickness of the

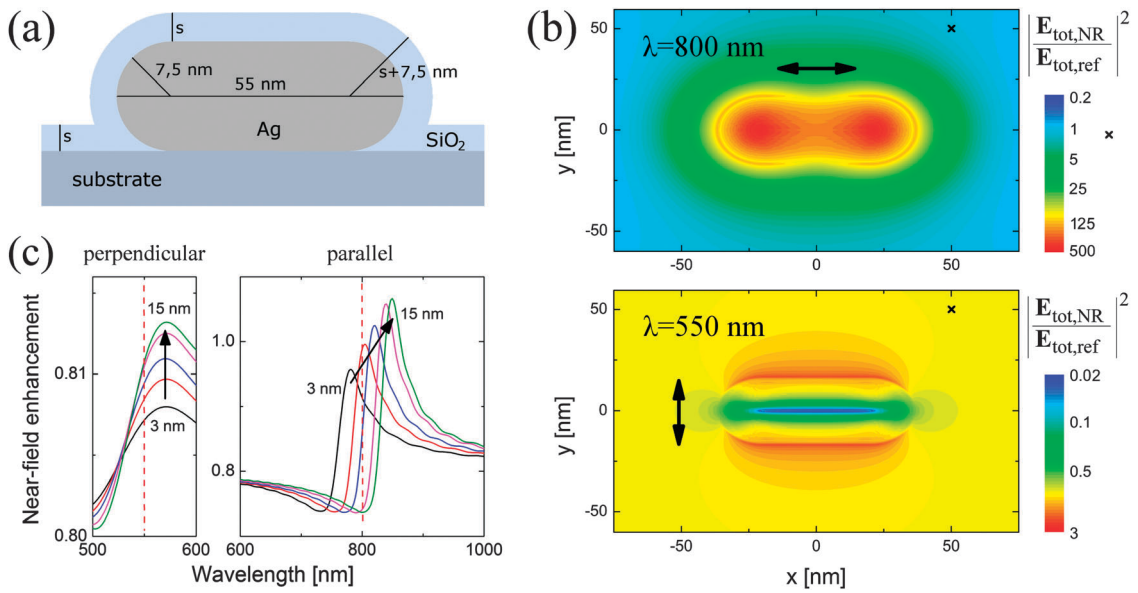

Fig. 5 (a) Schematic of the nanorod and the spacer structure considered for the calculations. (b) Maps of the electric field intensity enhancements $|\mathbf{E}_{\mathrm{tot,NR}}/\mathbf{E}_{\mathrm{tot,ref}}|^2$ calculated on the top of the spacer. The thickness of the spacer is set to s = 9 nm. The wavelength of the incident light is set at, respectively, 800 nm and 550 nm for the light polarized parallell (upper map) and perpendicular (lower panel) to the symmetry axis of the nanorod. The polarizations are marked by the black arrows. (c) Spectra of the near field enhancement calculated for spacer thickness varying from 5 nm to 13 nm for the incident light polarized perpendicular (left panel) or parallel (right panel) to the long axis of the nanorod. Black arrows indicate the shifting of the resonance position with increasing spacer thickness. Spectra are calculated for points marked in (b) with black crosses. Red dashed lines indicate the wavelengths of interest – 550 nm and 800 nm.

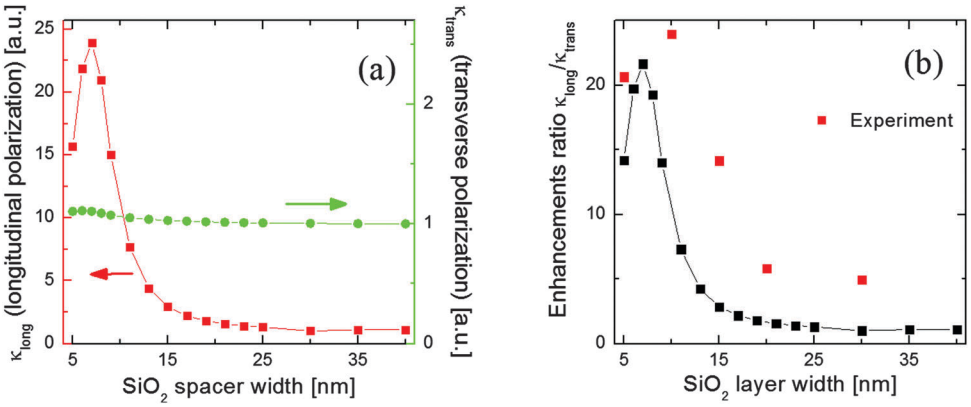

Fig. 6 (a) Enhancement factors as a function of spacer width for longitudinal (red squares) and transverse (green circles) nanorod polarization. (b) The ratio $\kappa_{long}/\kappa_{trans}$ of both enhancement parameters as a function of the spacer width. Lines are guide to eyes. Red points represent experimentally obtained values.

dielectric layer, and significantly redshifts from a wavelength of 800 nm (dashed red line) as the layers become thicker than 5 nm. In Fig. 6, we present the calculated enhancement factors κ_{trans} and κ_{long} as a function of the spacer width Fig. 6(a) and of their ratio $\kappa_{long}/\kappa_{trans}$ Fig. 6(b). The data in Fig. 6a correspond to the experimental results shown in the upper panel of Fig. 4. Specifically, the enhancement for the longitudinal polarization (red squares) in Fig. 6a peaks at around 7 nm and then decreases with an increasing spacer width. This behavior results from the redshift of the plasmon resonance with increasing spacer thickness, as illustrated in Fig. 5c. The spacer thickness which yields the maximum of κ_{long} is slightly smaller than that indicated by the experimental data (Fig. 4). This difference can be attributed to the imperfect coverage of the nanorod by the spacer, resulting in an effectively thicker dielectric layer.

The excitation enhancement for the transverse polarization (green circles in Fig. 6a) is much weaker and exhibits a small contribution from the scattering of the incident light on the nanorod for the thinnest layers. Since the spectral position of the transverse resonance depends weakly on the spacer thickness (left panel in Fig. 5c), we attribute the features of the rate enhancement plot to the purely geometric effects. The ratio of the excitation enhancements shown in Fig. 6b is similar to that revealed by the experimental results presented using red points in Fig. 6b, with the maximum of the ratio observed for the 7 nm dielectric layer (around 10 nm from the experimental results), followed by a quick decay for the thicker spacers. This discrepancy can be ascribed to the fact that the LH2 complexes are embedded in a PVA matrix. In this case the polymer will act the same way as the silica spacer, but its presence plays a role mainly for thinner spacers, as due to the narrow range of relevant plasmon interactions (below 20 nm) the actual enhancements would be blurred for spacers between 5 and 10 nm.

We can therefore attribute the dependence of the intensity of the enhancement ratio on the spacer thickness to the two aforementioned phenomena – the red-shifting of the longitudinal resonance with increasing spacer thickness and the very different spatial arrangement of the enhanced fields for the two resonant systems.

Conclusions

The results of confocal fluorescence mapping of hybrid nanostructures composed of light-harvesting photosynthetic complexes LH2 and Au nanorods indicate a strong dependence of the plasmon enhancement on the excitation wavelength. For the excitation resonant with transverse plasmon in the nanorods the enhancement is rather small (less than twofold) and exhibits weak dependence on the separation distance between both components of the nanostructures. In contrast, when the excitation is resonant with the longitudinal plasmon in the nanorods, the enhancement is more pronounced and reaches a maximum for the spacer thickness of around 10 nm. Experimental results are well reproduced by our theoretical modelling.

Acknowledgements

Research in Poland was supported by the WELCOME project "Hybrid Nanostructures as a Stepping Stone towards Efficient Artificial Photosynthesis" funded by the Foundation for Polish Science and EUROCORES project "BOLDCATS" funded by the European Science Foundation. Part of sample characterization measurements was carried out at the facilities of National Laboratory FAMO in the Institute of Physics, NCU in Torun. We thank Wojciech Zaleszczyk for performing SEM characterization of Au nanorods. THPB thanks the Indonesian Ministry of Research and Technology for SINAS Grant (RT-2012-0264) and the Indonesian Ministry of Education and Culture for the International Research Collaboration Grant (0541/023-04.1.01/00/2012). MKS and JA acknowledge funding from the ETORTEK project nanoiker of the Department of Industry of the Government of the Basque Country, project IT756-13 of the Department of Education and Culture of the Basque Country, scholarship AP-2012-4204 from the Spanish Ministry of Education,

Culture and Sport, and the project FIS2010-19609-C02-01 of the Spanish Ministry of Innovation.

References

1 S. A. Maier, *Plasmonics: Fundamentals and Applications*, Springer, 2010.
2 C.-C. Chen, L. Dou, R. Zhu, C.-H. Chung, T.-B. Song, Y. B. Zheng, S. Hawks, G. Li, P. S. Weiss and Y. Yang, *ACS Nano*, 2012, **6**, 7185–7190.
3 L. Novotny and N. van Hulst, *Nat. Photonics*, 2011, **5**, 83–90.
4 J. Lee, P. Hernandez, J. Lee, A. Govorov and N. Kotov, *Nat. Mater.*, 2007, **6**, 291–295.
5 H. K. Hunt and A. M. Armani, *Nanoscale*, 2010, **2**, 1544.
6 S. Mackowski, *J. Phys.: Condens. Matter*, 2010, **22**, 193102.
7 A. Polman and H. A. Atwater, *Nat. Mater.*, 2012, **11**, 174–177.
8 K. Kneipp, Y. Wang, H. Kneipp, L. T. Perelman, I. Itzkan, R. R. Dasari and M. S. Feld, *Phys. Rev. Lett.*, 1997, **78**, 1667–1670.
9 A. Hartschuh, H. N. Pedrosa, L. Novotny and T. D. Krauss, *Science*, 2003, **301**, 1354–1356.
10 S. Kühn, U. Håkanson, L. Rogobete and V. Sandoghdar, *Phys. Rev. Lett.*, 2006, **97**, 017402.
11 K.-S. Lee and M. A. El-Sayed, *J. Phys. Chem. B*, 2006, **110**, 19220–19225.
12 D. Aherne, D. M. Ledwith and J. M. Kelly, in *Metal-Enhanced Fluorescence*, ed. C. D. Geddes, John Wiley & Sons, Inc., 2010, pp. 295–362.
13 L. M. Liz-Marzán, *Langmuir*, 2005, **22**, 32–41.
14 G. W. Bryant, F. J. Garcia de Abajo and J. Aizpurua, *Nano Lett.*, 2008, **8**, 631–636.
15 Y. Fu, J. Zhang and J. R. Lakowicz, *J. Am. Chem. Soc.*, 2010, **132**, 5540–5541.
16 Y. Zhang, K. Aslan, M. J. R. Previte and C. D. Geddes, *PNAS*, 2008, **105**, 1798–1802.
17 K. Aslan, Z. Leonenko, J. R. Lakowicz and C. D. Geddes, *J. Phys. Chem. B*, 2005, **109**, 3157–3162.
18 T. Ming, L. Zhao, Z. Yang, H. Chen, L. Sun, J. Wang and C. Yan, *Nano Lett.*, 2009, **9**, 3896–3903.
19 R. E. Blankenship, *Molecular Mechanisms of Photosynthesis*, Blackwell Science, 1st edn, 2002.
20 S. Mackowski, S. Wormke, A. J. Maier, T. H. P. Brotosudarmo, H. Harutyunyan, A. Hartschuh, A. O. Govorov, H. Scheer and C. Brauchle, *Nano Lett.*, 2007, **8**, 558–564.
21 J. B. Nieder, R. Bittl and M. Brecht, *Angew. Chem., Int. Ed.*, 2010, **49**, 10217–10220.
22 S. R. Beyer, S. Ullrich, S. Kudera, A. T. Gardiner, R. J. Cogdell and J. Koehler, *Nano Lett.*, 2011, **11**, 4897–4901.
23 I. Carmeli, I. Lieberman, L. Kraversky, Z. Fan, A. O. Govorov, G. Markovich and S. Richter, *Nano Lett.*, 2010, **10**, 2069–2074.
24 L. Bujak, N. Czechowski, D. Piatkowski, R. Litvin, S. Mackowski, T. H. P. Brotosudarmo, R. J. Cogdell, S. Pichler and W. Heiss, *Appl. Phys. Lett.*, 2011, **99**, 173701.
25 C. Hoeppener and L. Novotny, *Q. Rev. Biophys.*, 2012, **45**, 209–255.
26 T. H. P. Brotosudarmo, R. Kunz, P. Böhm, A. T. Gardiner, V. Moulisová, R. J. Cogdell and J. Köhler, *Biophys. J.*, 2009, **97**, 1491–1500.
27 T. K. Sau and C. J. Murphy, *Langmuir*, 2004, **20**, 6414–6420.
28 B. Krajnik, T. Schulte, D. Piątkowski, N. Czechowski, E. Hofmann and S. Mackowski, *Cent. Eur. J. Phys.*, 2011, **9**, 293–299.
29 G. McDermott, S. Prince, A. Freer, N. Isaacs, M. Papiz, A. Hawthornthwaitelawless and R. Cogdell, *Protein Eng.*, 1995, **8**, 43.
30 A. M. van Oijen, M. Ketelaars, J. Kohler, T. J. Aartsma and J. Schmidt, *Science*, 1999, **285**, 400–402.
31 J. Kundu, F. Le, P. Nordlander and N. J. Halas, *Chem. Phys. Lett.*, 2008, **452**, 115–119.
32 J.-Y. Yan, W. Zhang, S. Duan, X.-G. Zhao and A. O. Govorov, *Phys. Rev. B: Condens. Matter Mater. Phys.*, 2008, **77**, 165301.
33 A. O. Govorov, G. W. Bryant, W. Zhang, T. Skeini, J. Lee, N. A. Kotov, J. M. Slocik and R. R. Naik, *Nano Lett.*, 2006, **6**, 984–994.
34 Lumerical Solutions, Inc. http://www.lumerical.com/tcad-products/fdtd/.
35 *Handbook of Optical Constants of Solids*, ed. E. D. Palik, Elsevier, 1998.

